TABLE OF CONTENTS

		Page	
I.	INTRODUCTION	1	1/A9
II.	EXACT SOLUTION	2	1/A10
III.	FIRST-ORDER APPROXIMATION	4	1/A12
	A. Single Surface Element	6	1/A14
	B. Combination of Two Elements	8	1/B2
IV.	THIRD-ORDER APPROXIMATION	11	1/B5
	A. Single Surface Element	13	1/B7
	B. Combination of Two Elements	17	1/B11
	C. Telescope	23	1/C3
V.	CONCLUSIONS	28	1/C8
REFERENCES		30	1/C10

LIST OF ILLUSTRATIONS

Figure	Title	Page	
1.	Forward reflection	5	1/A13
2.	Coma circle produced by single element working in grazing incidence	8	1/B2
3.	General two-element grazing incidence system	9	1/B3
4.	Three possible coordinate system choices for analyzing two-element grazing incidence optics: (a) a single system of coordinates centered in the plane of intersection of the two surfaces, (b) two systems of coordinates, one at the back of the first element and one at the front of the second element, and (c) two systems of coordinates, one centered on each element	12	1/B6
5.	Schematic of X-ray telescope	23	1/C3
6.	Spot sizes in the Gaussian image plane for three different off-axis angles	27	1/C7
7.	Exact spot size of image and spot size predicted by third-order theory versus off-axis angle	28	1/C8

NAS 1.60:1088

NOV 15 1977

NASA Technical Paper 1088

Performance Analysis of Grazing Incidence Imaging Systems

COMPLETED
ORIGINAL

Carl E. Winkler and Dietrich Korsch

NOVEMBER 1977

NASA

41

NAS 1.60: 1088

NASA Technical Paper 1088

Performance Analysis of Grazing Incidence Imaging Systems

Carl E. Winkler
George C. Marshall Space Flight Center
Marshall Space Flight Center, Alabama
and
Dietrich Korsch
Teledyne Brown Engineering
Huntsville, Alabama

National Aeronautics
and Space Administration

**Scientific and Technical
Information Office**

1977

LIST OF SYMBOLS

Symbol	Definition
A_1, A_2	Simplifications according to equations (52) and (53)
B, C, D, E, F	Coefficients of aberration terms
d	Distance between centers of the two optical elements
f	System focal length
k	Related to radius of curvature as discussed in Section III
m	Ratio of image distance to object distance
r	Radius of curvature
R_s	Radius of curvature of the saggital focal surface at the vertex
R_t	Radius of curvature of the tangential focal surface at the vertex
s	General object distance
s'	General image distance
s_1	Distance from object plane to center of first optical element
s_1'	Distance from center of first optical element to first image plane
s_2	Distance from first image plane to center of second optical element
s_2'	Distance from center of second optical element to final image plane for a two-element system
(x, y)	General off-axis surface coordinates
(x_1, y_1)	Off-axis surface coordinates on the first reflective surface

LIST OF SYMBOLS (Continued)

Symbol	Definition
(x_2, y_2)	Off-axis surface coordinates on the second reflective surface
z	Position along z-axis or optical axis
z_o	Position of surface vertex on optical axis
z_x	Partial derivative of z with respect to x
z_y	Partial derivative of z with respect to y
$1/R$	Field curvature
$\alpha_1, \beta_1, \gamma_1$	Direction cosines of incoming ray
$\alpha_2, \beta_2, \gamma_2$	Direction cosines of reflected ray
$\alpha_n, \beta_n, \gamma_n$	Direction cosines of surface normal
γ	Grazing angle between surface and incoming ray
γ_o	Off-axis angle between incoming ray and optical axis
δ	Deformation constant
$\Delta\xi_3, \Delta\eta_3$	Departure from perfect image
$\Delta\rho^2$	Difference between general surface radius squared and central radius squared
κ	Simplification according to equation (38)
ξ_r	Image position (reference)
(ξ_1, η_1)	Off-axis coordinates of a point in the object plane

LIST OF SYMBOLS (Concluded)

Symbol	Definition
(ξ_2, η_2)	Off-axis coordinates of a point in the image plane after a single reflection
(ξ_3, η_3)	Off-axis coordinates of a point in the image plane of a two-element system
τ	Radius of double circle in first image plane
ω	Angle that has y/ρ for its sine and x/ρ for its cosine
ρ	Radius of optical element
ρ_o	Radius of optical element at its center

PERFORMANCE ANALYSIS OF GRAZING INCIDENCE IMAGING SYSTEMS

I. INTRODUCTION

The purpose of this study is to systematically investigate general grazing incidence optical systems. Previous analytical work regarding grazing incidence has been restricted to two-mirror telescopes with a few selected aberrations [1-4]. A complete set of primary aberrations is developed here, and application to the design and optimization of grazing incidence systems is discussed [5,6]. Initial assumptions and approximations are explained, and the consequent limitations of the theory are presented. Since the wavelengths of X-rays are so short that diffraction effects are negligible, the geometric performance analysis of X-ray imaging systems is sufficiently representative and accurate.

An exact solution relating image coordinates to object coordinates following reflection from a single general surface of revolution is first developed [7]. These exact relations are then specialized for the case of grazing incidence which can be simply stated by requiring the angle between an incoming ray and a mirrored surface of revolution to be 1° or less. A first-order treatment shows that a single surface grazing incidence system results in a gross violation of the Abbe sine condition and that an even number of mirrors is required to achieve good imaging.

Finally, a third-order theory is developed that yields expressions for the primary aberrations: coma, spherical aberration, astigmatism, field curvature, and distortion. A simple relation for field curvature showing it to be the predominant aberration responsible for off-axis image degradation is the single most significant result of this study. It is also shown, to the accuracy of this theory, that a general two-element system displaying no spherical aberration is also free of coma. This is in good agreement with the fact that grazing incidence telescopes, when free of spherical aberration, are known to be very nearly aplanatic. A comparison of the findings with ray-trace results of a typical grazing incidence x-ray telescope design is included.

II. EXACT SOLUTION

The relation between a point on the incident ray, a point on the reflected ray, and the point of interception on the surface can be derived from the law of reflection:

$$\alpha_1 + \alpha_2 = 2\epsilon\alpha_n$$

$$\beta_1 + \beta_2 = 2\epsilon\beta_n \qquad (1)$$

$$\gamma_1 + \gamma_2 = 2\epsilon\gamma_n .$$

with

$$\epsilon = \alpha_1\alpha_n + \beta_1\beta_2 + \gamma_1\gamma_n \quad .$$

α_1, β_1, and γ_1 are the direction cosines of the incident ray; α_2, β_2, and γ_2 are the direction cosines of the reflected ray; and α_n, β_n, and γ_n are the direction cosines of the surface normal at the point of interception.

We divide equation (1) by γ_1 and get

$$(\alpha_2/\gamma_2)\ (\gamma_2/\gamma_1) = 2\alpha_n\epsilon/\gamma_1$$

$$(\beta_2/\gamma_2)\ (\gamma_2/\gamma_1) = 2\beta_n\epsilon/\gamma_1 \qquad (2)$$

$$(\gamma_2/\gamma_1) = 2\gamma_n\epsilon/\gamma_1 \quad .$$

Inserting the last of equation (2) into the first two then yields

$$\frac{\alpha_2}{\gamma_2} = \frac{(\alpha_1/\gamma_1) - 2\alpha_n\epsilon/\gamma_1}{1 - 2\gamma_n\epsilon/\gamma_1}$$

and (3)

$$\frac{\beta_2}{\gamma_2} = \frac{(\beta_1/\gamma_1) - 2\beta_n\epsilon/\gamma_1}{1 - 2\gamma_n\epsilon/\gamma_1} \quad .$$

Assuming a surface equation of the form $z = f(x,y)$ with the partial derivatives

$$z_x = \frac{\partial z}{\partial x} \qquad \text{and} \qquad z_y = \frac{\partial z}{\partial y} \quad ,$$

we have for the direction cosines of the surface normal:

$$\gamma_n = -1/(1 + z_x^2 + z_y^2)^{1/2} \quad ,$$

$$\alpha_n = -z_x\gamma_n \quad , \qquad (4)$$

$$\beta_n = -z_y\gamma_n \quad .$$

One can further express the ray directions by the coordinates of the initial point (ξ_1, η_1, s), the coordinates of the final point (ξ_2, η_2, s'), and the surface coordinates at the point of interception (x,y,z):

$$\alpha_1/\gamma_1 = (\xi_1 - x)/(s - z)$$

(5)
(Continued)

$$\beta_1/\gamma_1 = (\eta_1 - y)/(s - z)$$

$$\alpha_2/\gamma_2 = (\xi_2 - x)/(s' - z)$$

$$\beta_2/\gamma_2 = (\eta_2 - y)/(s' - z) \quad . \tag{5}$$

(Concluded)

Inserting equations (4) and (5) into equation (3) and solving for ξ_2 and η_2, respectively, finally gives

$$\xi_2 = [(W + \bar{s})(x - z_x\bar{s}') + (\bar{s}' - \bar{s})x - \bar{s}'\xi_1]/W \tag{6}$$

$$\eta_2 = [(W + \bar{s})(y - z_y\bar{s}') + (\bar{s}' - \bar{s})y - \bar{s}'\eta_1]/W \tag{7}$$

with

$$W = 2\gamma_n^2[z_x(x - \xi_1) + z_y(y - \eta_1) + \bar{s}] - \bar{s} \quad ,$$

and

$$\bar{s} = s - z \quad , \quad \bar{s}' = s' - z \quad .$$

III. FIRST-ORDER APPROXIMATION

While the portion around the vertex of a conicoid where the surface normal is nearly parallel to the axis of symmetry ($\gamma_n^2 \approx 1$) is conventionally used for imaging, we consider a portion of the same general type of surface at a distance from its vertex where the surface normal is almost orthogonal to the axis of symmetry, $\gamma_n^2 \ll 1$ (Fig. 1). This condition is true, for instance, for both elements in a Wolter-type X-ray telescope. The first-order approximation to be presented here shows some interesting results, differing significantly from those we get applying first-order or Gaussian optics to the near-normal incidence.

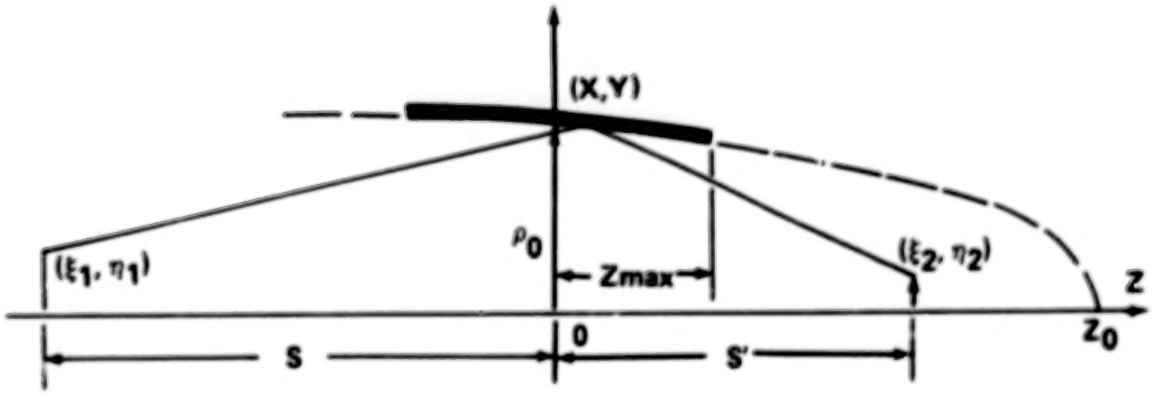

Figure 1. Forward reflection.

For the following application it is convenient to write the equation of a conicoid so that the origin coincides with the center of the portion under consideration:

$$\Delta\rho^2 = 2kz - (1+\delta)z^2 \quad , \tag{8}$$

where

$$\Delta\rho^2 = \rho^2 - \rho_0^2 \quad , \quad \rho^2 = x^2 + y^2 \quad , \quad \rho_0^2 = x^2 + y^2 \quad \text{for} \quad z = 0 \quad ,$$

and

$$k^2 = r^2 - (1+\delta)\,\rho_0^2 \quad ,$$

where r is the radius of curvature at the vertex and δ is the deformation constant. At the vertex of the conicoid ρ_0 equals 0, and k reduces to the radius of curvature.

Developing the surface equation with respect to z gives

$$z = \delta\rho^2/2k + [(1+\delta)/8k^3]\,(\Delta\rho^2)^2 + \ldots \quad ,$$

and the partial derivatives

$$z_x = x/k + [(1+\delta)/2k^3]\,\Delta\rho^2 x + \ldots \quad ,$$

$$z_y = y/k + [(1+\delta)/2k^3]\,\Delta\rho^2 y + \ldots \quad .$$

For our purpose it is sufficient to replace the surface equation and its derivatives by the first-order terms, i.e.,

$$z = 0 \quad , \quad z_x = x/k \quad , \quad z_y = y/k \quad ,$$

and consequently,

$$\gamma_n^2 = 1/(1 + z_x^2 + z_y^2) \approx k^2/(k^2 + \rho_0^2) \quad .$$

A. Single Surface Element

Inserting the previous terms into equation (6), we obtain

$$\xi_2 = \{\xi_1[2x^2(s'-k) - s'(k^2+\rho_0^2)] + \eta_1[2xy(s'-k)]$$

$$- x[2k(ss'-\rho_0^2) - (s+s')(k^2-\rho_0^2)]\}/W' \quad , \qquad (9)$$

with

$$W' = s(k^2-\rho_0^2) + 2k(\rho_0^2 - x\xi_1 - y\eta_1) \quad .$$

If we now require stigmatic imaging on axis, i.e.,

$$\xi_2 = \eta_2 = 0 \quad \text{for} \quad \xi_1 = \eta_1 = 0 \quad ,$$

we find that

$$2k(ss' - \rho_0^2) - (s + s')\,(k^2 - \rho_0^2) = 0 \quad , \tag{10}$$

which corresponds to the lens equation and assumes the conventional form for $\rho_0 = 0$. Equation (9) due to equation (10) reduces to

$$\xi_2 = \{\xi_1 [2x^2(s' - k) - s'(k^2 + \rho_0^2)] + \eta_1 [2xy(s' - k)]\}/W' \; . \tag{11}$$

Assuming that $\gamma_n^2 << 1$ and due to the requirement for grazing incidence, we may write

$$k << \rho_0 << |s|, \; |s'| \quad ,$$

which allows us to neglect k throughout equation (11). Retaining only first-order terms, equation (11) finally becomes

$$\xi_2 = -(1/\rho_0^2)\,(s'/s)\,[(2x^2 - \rho_0^2)\,\xi_1 + 2xy\eta_1] \quad , \tag{12}$$

and analogously

$$\eta_2 = -(1/\rho_0^2)\,(s'/s)\,[(2y^2 - \rho_0^2)\,\eta_1 + 2xy\xi_1] \quad . \tag{13}$$

That the last two equations are indeed of the first order becomes immediately apparent after replacing x and y by the polar coordinates:

$$x = \rho_0 \cos\phi \qquad \text{and} \qquad y = \rho_0 \sin\phi \quad .$$

Setting further $\eta_1 = 0$, which may be done without losing generality, we get for equations (12) and (13):

$$\xi_2 = -(s'/s)\xi_1\,(2\cos^2\phi - 1) = -(s'/s)\xi_1 \cos 2\phi = \tau \cos 2\phi \quad , \tag{14}$$

$$\eta_2 = -(s'/s)\xi_1\ 2\sin\phi\ \cos\phi = -(s'/s)\xi_1\ \sin 2\phi = \tau \sin 2\phi \quad . \qquad (15)$$

Equations (14) and (15) describe a circle in the image plane centered on-axis with the radius τ and an amplitude of 2ϕ which is twice the amplitude at the surface (Fig. 2).

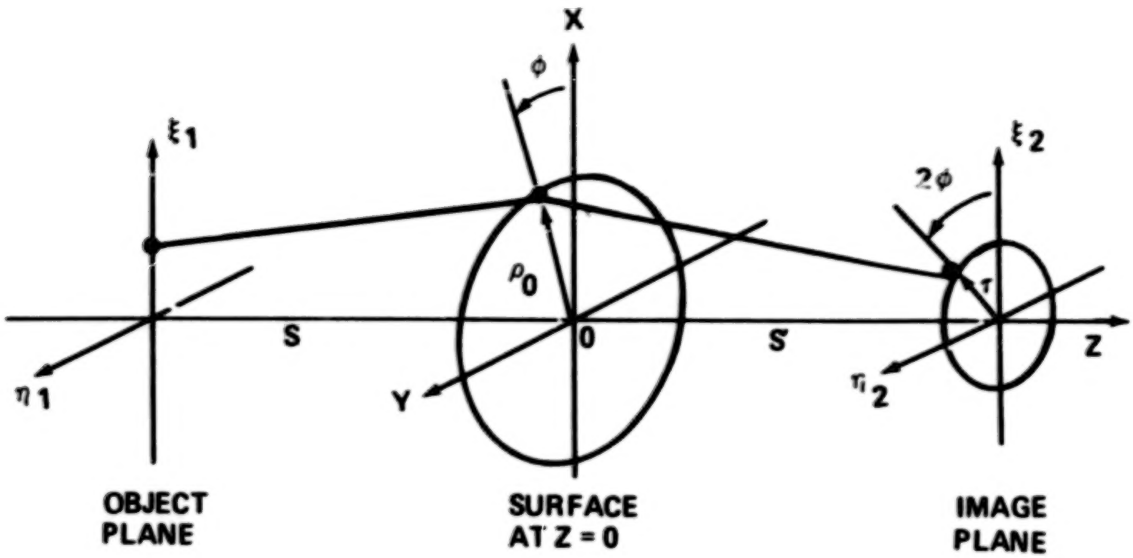

Figure 2. Coma circle produced by single element working in grazing incidence.

B. Combination of Two Elements

Let us now combine two elements, both working in grazing incidence as schematically shown in Figure 3. The subscripts 1 on x, y, ρ, s and s' refer to the first surface element and the subscripts 2 to the second. For simplicity, we again set $\eta_1 = 0$. We then get, for the coordinates in the image plane of the first element,

$$\xi_2 = -(\xi_1/\rho_{01}^2)\ (s_1'/s_1)\ (2x_1^2 - \rho_{01}^2) \quad , \qquad (16)$$

$$\eta_2 = -(\xi_1/\rho_{01}^2)\ (s_1'/s_1)\ 2x_1\ y_1 \quad , \qquad (17)$$

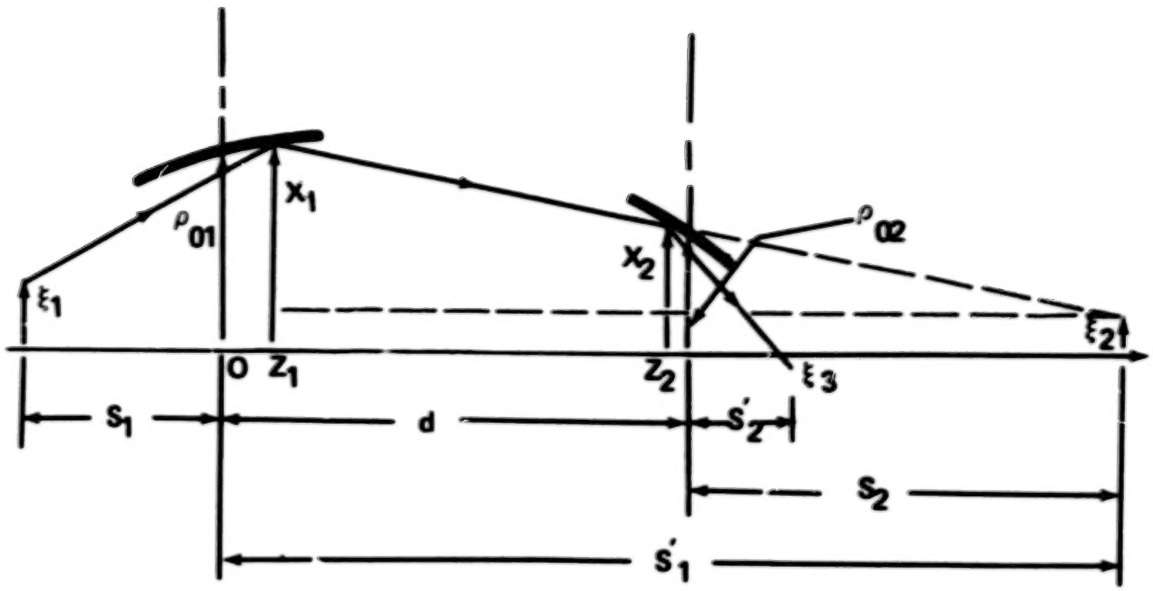

Figure 3. General two-element grazing incidence system.

and in the image plane of the second element,

$$\xi_3 = -\frac{1}{\rho_{02}^2}\frac{s'_2}{s_2}\left[(2x_2^2 - \rho_{02}^2)\xi_2 + 2x_2\, y_2\, \eta_2\right] \quad , \tag{18}$$

$$\eta_3 = -\frac{1}{\rho_{02}^2}\frac{s'_2}{s_2}\left[(2y_2^2 - \rho_{02}^2)\,\eta_2 + 2x_2\, y_2\, \xi_2\right] \quad . \tag{19}$$

Since the object and image coordinates are assumed to be small quantities, we have the following simple first-order relations between the ray coordinates on the first and the second surface:

$$x_2 = x_1\, s_2/s'_1 \quad , \quad y_2 = y_1\, s_2/s'_1 \quad , \quad \rho_{02} = \rho_{01}\, s_2/s'_1$$

inserted into equation (18) gives

$$\xi_3 = \frac{\xi_1}{\rho_{01}^4}\frac{s'_1\, s'_2}{s_1\, s_2}\left(4x_1^4 - 4x_1^2\,\rho_{01}^2 + \rho_{01}^4 + 4x_1^2 y_1^2\right) \quad , \tag{20}$$

and using

$$y_1^2 = \rho_{01}^2 - x_1^2$$

yields

$$\xi_3 = \xi_1 \frac{s_1' s_2'}{s_1 s_2} \quad . \tag{21}$$

In the case of a telescope, setting

$$s_2'/s_2 = m_2$$

and

$$\xi_1/s_1 = \gamma_0 \quad ,$$

γ_0 being the field angle, one obtains

$$\xi_3 = s_1' m_2 \gamma_0 \quad , \tag{22}$$

where

$$\xi_3/\gamma_0 = m_2 s_1' = f$$

is the system focal length.

Similarly, for η_3 we get

$$\eta_3 = \frac{\xi_1}{\rho_{01}^4} \frac{s_1' s_2'}{s_1 s_2} [(2y_1^2 - \rho_{01}^2) 2x_1 y_1 + 2x_1 y_1 (2x_1^2 - \rho_{01}^2)] \quad . \tag{23}$$

Again using

$$y_1^2 = \rho_{01}^2 - x_1^2 \quad ,$$

we have

$$\eta_3 = 0 \quad . \tag{24}$$

The significance of equations (21) and (24) is that contrary to a single element, any two-mirror system, as long as it fulfills the condition for grazing incidence, shows no dependence on the surface coordinates and thus is able to image off-axis points or field angles.

We may now further conclude that, since after two reflections the image of a point is approximately a point again, a third mirror would produce the same image as does a single element, i.e., systems working in grazing incidence are useful imaging devices only when consisting of an even number of elements.

IV. THIRD-ORDER APPROXIMATION

While the result of an exact theory is coordinate independent, the accuracy of an approximation usually is a function of the coordinates. The center of highest accuracy in aberration theories, for instance, generally coincides with $z = 0$, where the z-axis is the optical axis. In this case, the analytical result depends very definitely on the location of the origin with respect to the optical surface.

Figure 4 shows the same two-element grazing incidence system three times with three differently placed systems of coordinates. Figure 4a shows a single system of coordinates centered in the plane of intersection of the two surfaces. We do not regard this as the optimum position because, in a real system, the surface portions in the vicinity of the intersection do not exist. The second example (Fig. 4b) has two systems of coordinates, one at the back end of the first element and one at the front end of the second element. Since an end section is the least representative portion of the entire surface, we do not think that this choice is a significant improvement over the first case. We therefore selected the system depicted in Figure 4c, where the origins of two systems of coordinates coincide with the center of each individual element.

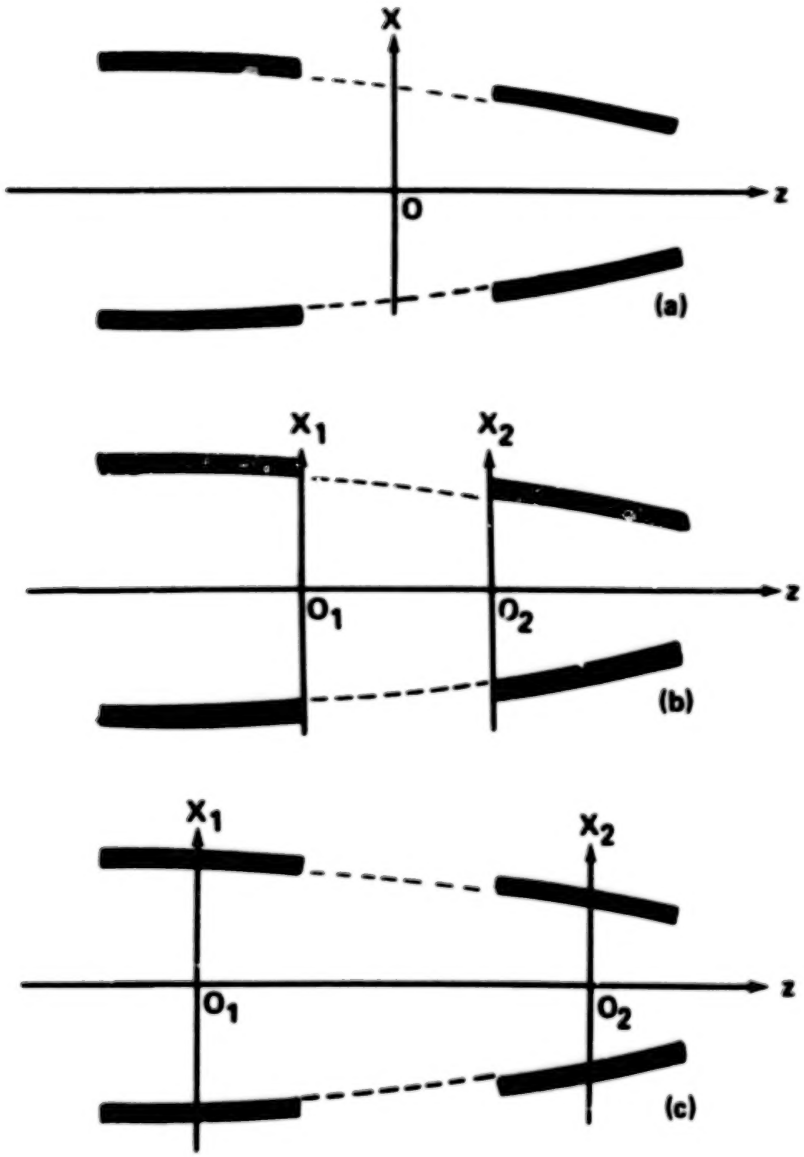

Figure 4. Three possible coordinate system choices for analyzing two-element grazing incidence optics: (a) a single system of coordinates centered in the plane of intersection of the two surfaces, (b) two systems of coordinates, one at the back of the first element and one at the front of the second element, and (c) two systems of coordinates, one centered on each element.

We shall later show that the result justifies our choice. Only the configuration in Figure 4c allows us to predict the correct amount of field curvature, the predominant aberration of two-element grazing incidence systems; and,

since the field curvature depends linearly on the distance between the origins, pushing the two origins toward the intersection plane leads to the illusion of a disappearing field curvature caused by a mere transformation of coordinates.

With this preamble behind us we now proceed to develop a primary or third-order aberration theory for grazing incidence.

A. Single Surface Element

The starting point for the development of the single surface aberrations is again the exact relations between object and image coordinates as given by equations (6) and (7), where ξ_1, η_1, and ε are the coordinates of a point on the incident ray; ξ_2, η_2, and s' are the coordinates of a point on the reflected ray; x, y, and z are the coordinates of the point of interception on the surface; and z_x and z_y are the partial derivatives of the surface equation $z = f(x,y)$ at the point of interception. The surface equation describing a general surface of revolution is given by equation (8).

Before we apply any approximation necessary to expand equations (6) and (7), and because of the obvious differences between grazing incidence and near-normal incidence, let us consider the relative order of magnitude of the involved quantities. The angle between ray and surface tangent for grazing incidence is of the order of 1° or less (<0.02 rad). We then obtain for the surface slopes:

$$\left.\begin{aligned} x_z &= [k - (1+\delta)z]/x \\ y_z &= [k - (1+\delta)z]/y \end{aligned}\right\} \ll 1 \qquad (25)$$

and in particular for the slope at the center (z = 0)

$$k/\rho_0 \ll 1 \quad . \qquad (26)$$

Existing proven telescope designs where the length of the reflecting element is approximately equal to its diameter allow us to make the further assumption that $z_{max} \approx x_{max} \approx \rho_0$ (Fig. 1). It follows, then, that

$$1 + \delta \ll 1 \quad . \qquad (27)$$

The main difference between near-normal and grazing incidence is that while in the case of near-normal incidence:

$$\left.\begin{matrix} z_x \\ z_y \end{matrix}\right\} \ll 1 \quad , \tag{28}$$

in the case of grazing incidence, we have

$$\left.\begin{matrix} x_z \\ y_z \end{matrix}\right\} \ll 1 \quad . \tag{29}$$

From the inequality of equation (27), we may furthermore conclude that for grazing incidence

$$\delta \approx -1 \quad , \tag{30}$$

i.e., the surface is always closely described by a paraboloid.

Solving the surface equation (8) for z and developing with respect to $\Delta\rho^2$ gives

$$z \approx \Delta\rho^2/2k + (1 + \delta)\,(\Delta\rho^2)^2/8k^3 \quad . \tag{31}$$

The partial derivatives with respect to x and y are

$$z_x \approx x/k + (1 + \delta)\,\Delta\rho^2 x/2k^3 \tag{32}$$

and

$$z_y \approx y/k + (1 + \delta)\,\Delta\rho^2 y/2k^3 \quad . \tag{33}$$

We restrict our analysis to the vicinity of $z = 0$ at each surface. To this end, we neglect all terms containing $(\Delta\rho^2)^n$ with $n > 1$. Obeying this basic rule, after inserting equations (31) through (33) into equations (6) and (7) and applying also the imaging equation for grazing incidence [equation (10)], and using the relation

$$m = s'/s \quad , \tag{34}$$

we find that

$$\xi_2 = \left\{ -\frac{2s'}{m+1}\left[1 - \frac{s'(m+1)(1+\delta)}{2km}\right] x\frac{\Delta\rho^2}{\rho_0^2} + s'\left[\frac{2x}{\rho_0^2}\kappa - \xi_1\right] \right.$$

$$\left. -\frac{m^2-1}{2s'}x\kappa + \frac{s'}{m+1}\left[\frac{2x}{\rho_0^2}\kappa - \xi_1\right]\frac{\Delta\rho^2}{\rho_0^2} \right\} / W \quad , \tag{35}$$

$$\eta_2 = \left\{ -\frac{2s'}{m+1}\left[1 - \frac{s'(m+1)(1+\delta)}{2km}\right] y\frac{\Delta\rho^2}{\rho_0^2} + s'\left[\frac{2y}{\rho_0^2}\kappa - \eta_1\right] \right.$$

$$\left. -\frac{m^2-1}{2s'}y\kappa + \frac{s'}{m+1}\left[\frac{2y}{\rho_0^2}\kappa - \eta_1\right]\frac{\Delta\rho^2}{\rho_0^2} \right\} / W \quad , \tag{36}$$

and

$$\frac{1}{W} = -\frac{m}{s'}\left[1 - \frac{\rho_0^2(m^2-1)}{2s'^2} + \frac{m(m+1)}{s'^2}\kappa + \frac{m}{(m+1)}\frac{\Delta\rho^2}{\rho_0^2}\right] \quad . \tag{37}$$

In the above

$$\kappa = (\xi_1 x + \eta_1 y) \quad , \tag{38}$$

and we have used the approximate value for k from equation (10),

$$k \approx -\rho_0^2 (s + s') / 2ss' \quad , \tag{39}$$

whenever this could be done without losing accuracy. Substitution of equation (37) into equations (35) and (36) yields

$$\xi_2 = m\xi_1 - \frac{2m}{\rho_0^2} x\kappa + \frac{4m^2}{\rho_0^4} x\kappa\Delta\rho^2 - \frac{m(m-1)}{\rho_0^2(m+1)} \xi_1 \Delta\rho^2$$

$$+ \frac{m}{\rho_0^2 (m+1)} \left[1 - \frac{s'(m+1)(1+\delta)}{2km} \right] x\Delta\rho^2$$

$$- \frac{2m^2(m+1)}{\rho_0^2 s'^2} x\kappa^2 + \frac{m^2(m+1)}{s'^2} \kappa \xi_1 \tag{40}$$

and

$$\eta_2 = m\eta_1 - \frac{2m}{\rho_0^2} y\kappa + \frac{4m^2}{\rho_0^4} y\kappa\Delta\rho^2 - \frac{m(m-1)}{\rho_0^2 (m+1)} \eta_1 \Delta\rho^2$$

$$+ \frac{m}{\rho_0^2 (m+1)} \left[1 - \frac{s'(m+1)(1+\delta)}{2km} \right] y\Delta\rho^2$$

$$- \frac{2m^2(m+1)}{\rho_0^2 s'^2} y\kappa^2 + \frac{m^2 (m+1)}{s'^2} \kappa\eta_1 \quad . \tag{41}$$

Setting $\xi_2 = \eta_2 = 0$ for $\xi_1 = \eta_1 = 0$ in either equation (40) or (41) yields the condition that must be met to remove spherical aberration,

$$\delta = \frac{2k}{s+s'} - 1 \quad . \tag{42}$$

Equations (40) and (41) contain the primary aberrations for a single-element system. The second term in each of these equations produces the large coma effect that characterizes such systems, as shown previously by Figure 2.

B. Combination of Two Elements

A two-element grazing incidence system is shown in Figure 3. To differentiate between the two surfaces, we have introduced the subscripts 1 and 2. The first surface is further characterized by the parameters k_1 and δ_1, and the second surface by k_2 and δ_2. In this system, an object point (ξ_1, η_1) at a distance s_1 from the center of the first element is imaged into (ξ_3, η_3) a distance s_2' from the center of the second element, separated from the first by a distance d. This report specifically concerns the case of a telescope; however, it should be noted that applications to systems other than telescopes also obey the theory developed here.

Considering (ξ_2, η_2) to be a source point for the second surface, the image point is then located at (ξ_3, η_3). Following equations (40) and (41) but eliminating the last two terms in each since they are small compared to the first two terms,

$$\xi_3 = \frac{m_2}{\rho_{02}^2}\left[1 - \frac{2m_2}{m_2+1}\,\Delta\rho_2^2\right]\left[(y_2^2 - x_2^2)\,\xi_2 - 2x_2y_2\eta_2\right]$$

$$+ \frac{2m_2}{\rho_{02}^2(m_2+1)}\left[1 - \frac{s_2'(m_2+1)(1+\delta_2)}{2k_2m_2}\right]\Delta\rho_2^2 x_2 \qquad (43)$$

and

$$\eta_3 = \frac{m_2}{\rho_{02}^2}\left[1 - \frac{2m_2}{m_2+1}\,\Delta\rho_2^2\right]\left[(x_2^2 - y_2^2)\,\eta_2 - 2x_2y_2\xi_2\right]$$

$$+ \frac{2m_2}{\rho_{02}^2(m_2+1)}\left[1 - \frac{s_2'(m_2+1)(1+\delta_2)}{2k_2m_2}\right]\Delta\rho_2^2 y_2 \quad . \qquad (44)$$

To write expressions for ξ_3 and η_3 in terms of ξ_1, $\Delta\rho_1^2/\rho_{01}^2$, x_1 and y_1, we need to develop relations between second and first surface coordinates. Referring to Figure 3, it can be seen that

$$\frac{s_1' - z_1}{s_2 - z_2} = \frac{x_1 - \xi_2}{x_2 - \xi_2} = \frac{y_1 - \eta_2}{y_2 - \eta_2} \tag{45}$$

and

$$\rho_{02} = \rho_{01} \frac{s_2}{s_1}$$

Again, setting $\eta_1 = 0$, which we can do without losing generality, we find to the desired accuracy that

$$\frac{x_2}{\rho_{02}} = \frac{x_1}{\rho_{01}} + \frac{m_1 d}{\rho_{01}^3 s_2} \left[(y_1^2 - x_1^2) + \frac{2m_2}{m_2 - 1} x_1^2 \right] \xi_1 \quad , \tag{46}$$

$$\frac{y_2}{\rho_{02}} = \frac{y_1}{\rho_{01}} - \frac{m_1 d}{\rho_{01}^3 s_2} \left[2x_1 y_1 - \frac{2m_2}{m_2 - 1} x_1 y_1 \right] \xi_1 \quad , \tag{47}$$

$$\begin{aligned} \frac{y_2^2 - x_2^2}{\rho_{02}^2} = {} & (y_1^2 - x_1^2) \left[\frac{1}{\rho_{01}^2} - \frac{2(m_1 m_2 - 1)}{\rho_{01}^4 (m_1 + 1)(m_2 - 1)} \Delta\rho_1^2 \right] \\ & - \frac{2m_1 d}{\rho_{01}^4 s_2} \left[(3y_1^2 - x_1^2) - \frac{2m_2}{m_2 - 1} (y_1^2 - x_1^2) \right] x_1 \xi_1 \\ & + \frac{m_1^2 d^2}{\rho_{01}^4 s_2^2} \left[(2x_1 y_1)^2 - \rho_{01}^2 (y_1^2 - x_1^2) \right] \xi_1^2 \quad , \end{aligned} \tag{48}$$

$$\frac{2x_2y_2}{\rho_{02}^2} = 2x_1y_1\left[\frac{1}{\rho_{01}^2} - \frac{2(m_1m_2-1)}{\rho_{01}^4(m_1+1)(m_2-1)}\Delta\rho_1^2\right]$$

$$+\frac{2m_1d}{\rho_{01}^4 s_2}\left[(y_1^2-3x_1^2) - \frac{2m_2}{m_2-1}x_1^2\right]y_1\xi_1$$

$$-\frac{m_1^2d^2}{\rho_{01}^6 s_2^2}\left[4x_1y_1(y_1^2-x_1^2)\right]\xi_1^2 \qquad (49)$$

and

$$\frac{\Delta\rho_2^2}{\rho_{02}^2} = -\frac{(m_2+1)(m_1-1)}{\rho_{01}^2(m_1+1)(m_2-1)} + \frac{2m_1(m_2+1)d}{\rho_{01}^2 s_2(m_2-1)}x_1\xi_1$$

$$+\frac{m_1^2(m_2+1)d^2}{\rho_{01}^2 s_2^2(m_2-1)}\xi_1^2 \quad . \qquad (50)$$

Substituting equations (40) and (41), with the proper subscripts, and equations (46) through (50) into equations (42) and (44), we obtain

$$\xi_3 = m_1m_2\xi_1 - \frac{2}{\rho_{01}^2(m_1+1)}\left[A_1m_2+A_2\frac{s_2(m_1-1)}{s_1^2(m_2-1)}\right]\Delta\rho_1^2x_1$$

$$+\frac{4m_1dA_2}{\rho_{01}^2 s_1^2(m_2-1)}x_1^2\xi_1 - \frac{2m_1^2m_2d}{\rho_{01}^2 s_2}\left[1+\frac{dA_2}{s_1^2 m_2(m_2-1)} - \frac{\rho_{01}^2 s_2(m_1+1)}{2ds_1^2}\right]x_1\xi_1^2$$

$$-\frac{2m_1^3m_2^2(m_2+1)d^2}{\rho_{01}^2 s_2^2(m_1+1)(m_2-1)}\xi_1^3 \qquad (51)$$

and

$$\eta_3 = -\frac{2}{\rho_{01}^2 (m_1+1)} \left[A_1 m_2 + A_2 \frac{s_2 (m_1-1)}{s_1' (m_2-1)} \Delta\rho_\cdot^2 y_1 \right]$$

$$+ \frac{4 m_1 dA_2}{\rho_{01}^2 s_1' (m_2-1)} x_1 y_1 \xi_1$$

$$- \frac{2 m_1^2 m_2 d}{\rho_{01}^2 s_2} \left[1 + \frac{dA_2}{s_1' m_2 (m_2-1)} \right] y_1 \xi_1^2 \quad , \tag{52}$$

where

$$A_1 = m_1 - \frac{s_1' (m_1+1)(1+\delta_1)}{2k_1} \tag{53}$$

and

$$A_2 = m_2 - \frac{s_2' (m_2+1)(1+\delta_2)}{2k_2} \quad . \tag{54}$$

Again, we have used equation (39), the approximate form of the imaging equation, in writing equations (51) and (52); however, equations (53) and (54) are exact relations, providing for $A_1 = A_2 = 0$ the deformation constants δ_1 and δ_2 for a system that is rigorously free of spherical aberration.

An analysis of equations (51) and (52) shows that an off-axis point located at $(\xi_1, 0, s_1)$ is imaged into a position $(m_1 m_2 \xi_1, 0, d + s_2')$. If we now, as is usually done, designate the linear term $m_1 m_2 \xi_1 = \xi_r$ as reference point for the image location, then the remaining terms, describing the departure from that point, form the aberration terms. Using Schwarzschild's notation [8] for aberration coefficients, we obtain

$$\Delta\xi_3 = \xi_3 - \xi_r$$

$$= B\Delta\rho_1^2 x_1 + Fx_1^2\xi_1 + (2C+D)x_1\xi_1^2 + E\xi_1^3 \qquad (55)$$

and

$$\Delta\eta_3 = \eta_3 = B\Delta\rho_1^2 y_1 + Fx_1 y_1 \xi_1 + Dy_1\xi_1^2 \quad . \qquad (56)$$

In general, the coefficients B, C, D, E, and F have finite values, and each term then represents a particular type of departure from perfect imaging. From equations (51), (52), (55), and (56), we can write

$$B = -\frac{2}{\rho_{01}^2(m_1+1)}\left[A_1 m_2 + A_2\frac{s_2(m_1-1)}{s_1'(m_2-1)}\right] \qquad (57)$$

$$F = \frac{4m_1 dA_2}{\rho_{01}^2 s_1'(m_2-1)} \qquad (58)$$

$$C = -\frac{m_1^2 m_2 d}{\rho_{01}^2 s_2}\left[-\frac{\rho_{01}^2 s_2(m_1+1)}{2ds_1'^2}\right] \qquad (59)$$

$$D = -\frac{2m_1^2 m_2 d}{\rho_{01}^2 s_2}\left[1 + \frac{dA_2}{s_1' m_2(m_2-1)}\right] \qquad (60)$$

$$E = -\frac{2m_1^3 m_2^2(m_2+1)d^2}{\rho_{01}^2 s_2^2(m_1+1)(m_2-1)} \quad . \qquad (61)$$

A system free of spherical aberration ($A_1 = A_2 = 0$) is also, to the accuracy of this theory, free of coma according to equation (58). This is in

agreement with grazing incidence x-ray telescope designs which are known to be very nearly aplanatic [1]. We also find that $|E| << |D|$ by inspection of equations (60) and (61). Distortion is not significant in these systems. The two remaining primary aberrations, astigmatism and field curvature, can be separated in the conventional manner:

$$1/2R_s = Ds_1' / m_1^2 m_2 \tag{62}$$

$$1/2R_t = (2C+D)s_1' / m_1^2 m_2 \quad , \tag{63}$$

where R_s and R_t are the radii of curvature at the vertex of the saggital and tangential focal surfaces, respectively. The field curvature is given by the arithmetic mean:

$$1/R = 1/2R_s + 1/2R_t = 2(C+D)s_1' / m_1^2 m_2 \quad , \tag{64}$$

and astigmatism is found from the semi-difference:

$$1/2R_t - 1/2R_s = 2Cs_1' / m_1^2 m_2 \quad . \tag{65}$$

Since $|C| << |D|$, field curvature is the predominant aberration and is given by

$$\frac{1}{R} \approx \frac{2Ds_1'}{m_1^2 m_2} = - \frac{4s_1' d}{\rho_{01}^2 s_2} \tag{66}$$

for the aplanatic system.

Equation (66) shows that increasing the diameter of the elements would decrease the effect of field curvature; but, to maintain grazing incidence conditions, the image distance would rapidly increase, causing instrument manufacturing difficulties. Decreasing d would decrease field curvature; however, the collecting area would be sacrificed. Some reduction in the effect of field curvature can be achieved by introducing small amounts of spherical aberration in the proper direction according to equations (57) and (60).

C. Telescope

Consider a telescope with zero spherical aberration such as used in X-ray astronomy [9-14]. Figure 5 shows a typical instrument schematically. Such a system will be designed in this section by specifying the radius of the first mirrored element, the distance between the two elements, and the grazing angle at the center of each element.

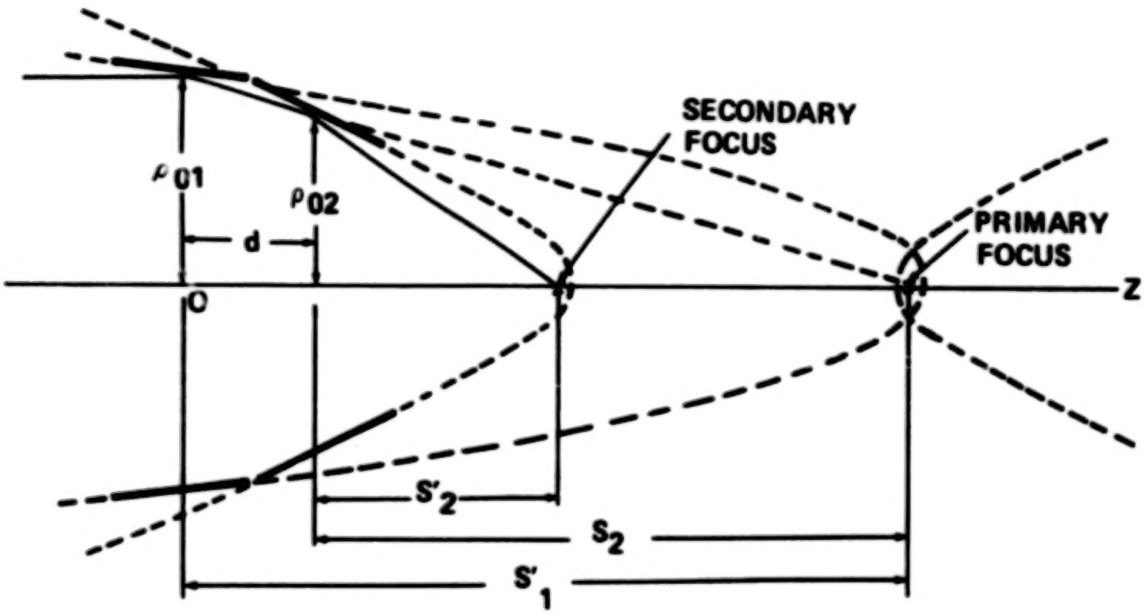

Figure 5. Schematic of X-ray telescope.

From equation (53) $\delta_1 = -1$; that is, the first surface is a paraboloid of revolution. At $\rho_1 = 0$, equation (8) gives

$$z = z_0 = -\rho_{01}^2 / 2k_1 \quad . \tag{67}$$

Then we have for the first surface image distance

$$s_1' = z_0 + k_1/2 \quad , \tag{68}$$

where $k_1/2$ is the distance between the vertex located at $z = z_0$ and the focal point of the paraboloid.

The image from the initial reflection can be regarded as the object for the second reflection; therefore,

$$s_2 = s_1' - d \quad . \tag{69}$$

The radius at the center of the second element can be found from $\rho_{02} = \rho_{01}\, s_2/s_1'$. Taking the grazing angle at the center of each element to be γ, the angle between the final ray and the optical axis is 4γ. Therefore, the distance from the center of the second element to the focal plane for the system is

$$s_2' = \rho_{02}/\tan 4\gamma \quad . \tag{70}$$

Since the incoming ray is parallel to the z-axis, we have

$$k_1 = -\rho_{01} \tan \gamma \tag{71}$$

and

$$k_2 = -\rho_{02} \tan 3\gamma \quad . \tag{72}$$

Starting with the following specified values

$\gamma = 1°$

$\rho_{01} = 10$ U. L.

$d = 20$ U. L. ,

where U. L. signifies units of length, we can generate a typical X-ray telescope design. We find that

$s_1' = 286.3625328$ U.L.

$s_2 = 266.3625328$ U.L.

$\rho_{02} = 9.30158461$ U.L.

$s_2' = 133.0188572$ U.L.

$m_2 = 0.499390270$

$k_1 = -0.174550649$ U.L.

$k_2 = -0.487475393$ U.L.

To make the system aplanatic to the third order, we specify $A_2 = 0$ in equation (54). Calculating the deformation constant for the second surface, we find that

$$\delta_2 = -1.002441152 \quad .$$

For the case of a telescope, we set $\xi_1 = \gamma_0 s_1' / m_1$, with γ_0 being the off-axis angle. Then for the off-axis image position, $\xi_3 = m_1 m_2 \xi_1$, we have

$$\xi_3 = s_1' m_2 \gamma_0 \quad , \tag{73}$$

with $\xi_3 / \gamma_0 = s_1' m_2$ being the system focal length f. For the telescope under consideration,

$$f = 143 \text{ U.L.} \quad .$$

Writing equations (55) and (56) for an aplanatic telescope with negligible distortion and astigmatism, one obtains

$$\Delta\xi_3 \approx -\gamma_0^2 x_1 \frac{2m_2 ds_1'^2}{\rho_{01}^2 s_2} \tag{74}$$

and

$$\Delta\eta_3 \approx -\gamma_0^2 y_1 \frac{2m_2 ds_1'^2}{\rho_{01}^2 s_2} \quad . \tag{75}$$

From equation (66), the field curvature is

$$\frac{1}{R} = -0.8601$$

which agrees rather well with the exact field curvature -0.8654 determined by ray-trace methods.

In Figure 6, the dots represent the points of intersection of 32 rays with the Gaussian image plane. Incoming parallel rays at an off-axis angle, γ_0, with respect to the z-axis strike the first surface in equally space points around the ring at $z = 0$. The circular patterns predicted by equations (74) and (75) agree quite well with the dot patterns as shown by Figure 6 for three different off-axis angles.

A plot of maximum image spot diameter as a function of off-axis angle (Fig. 7) shows close agreement between the exact spot size and that predicted from primary aberrations. As the off-axis angle is increased, the theoretical and actual spot diameters gradually move apart with an approximate departure error of 10 percent for an off-axis angle of 15 min of arc.

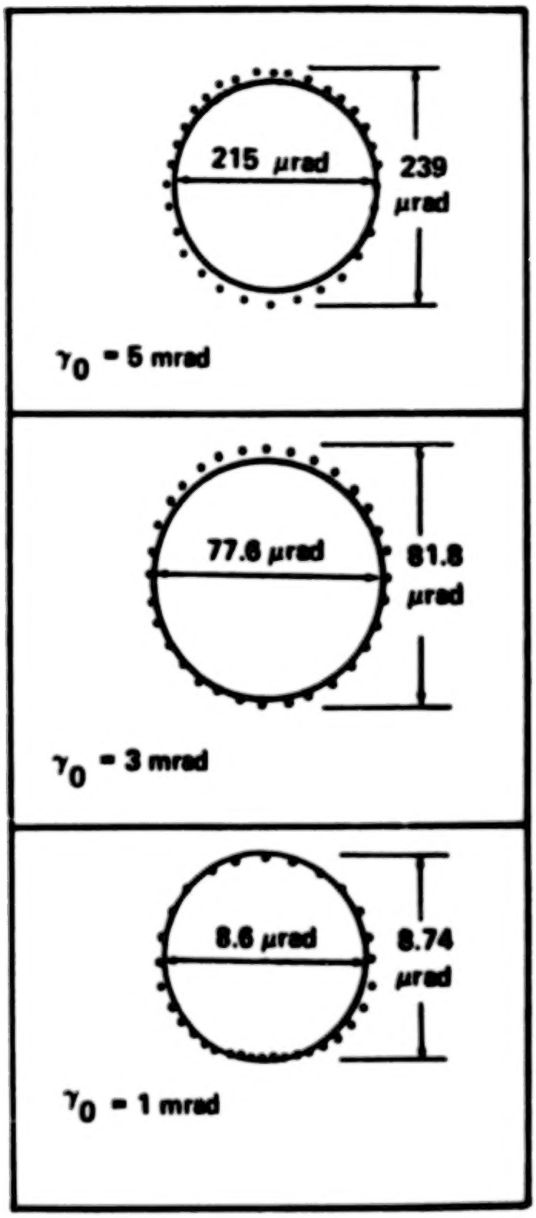

Figure 6. Spot sizes in the Gaussian image plane for three different off-axis angles.

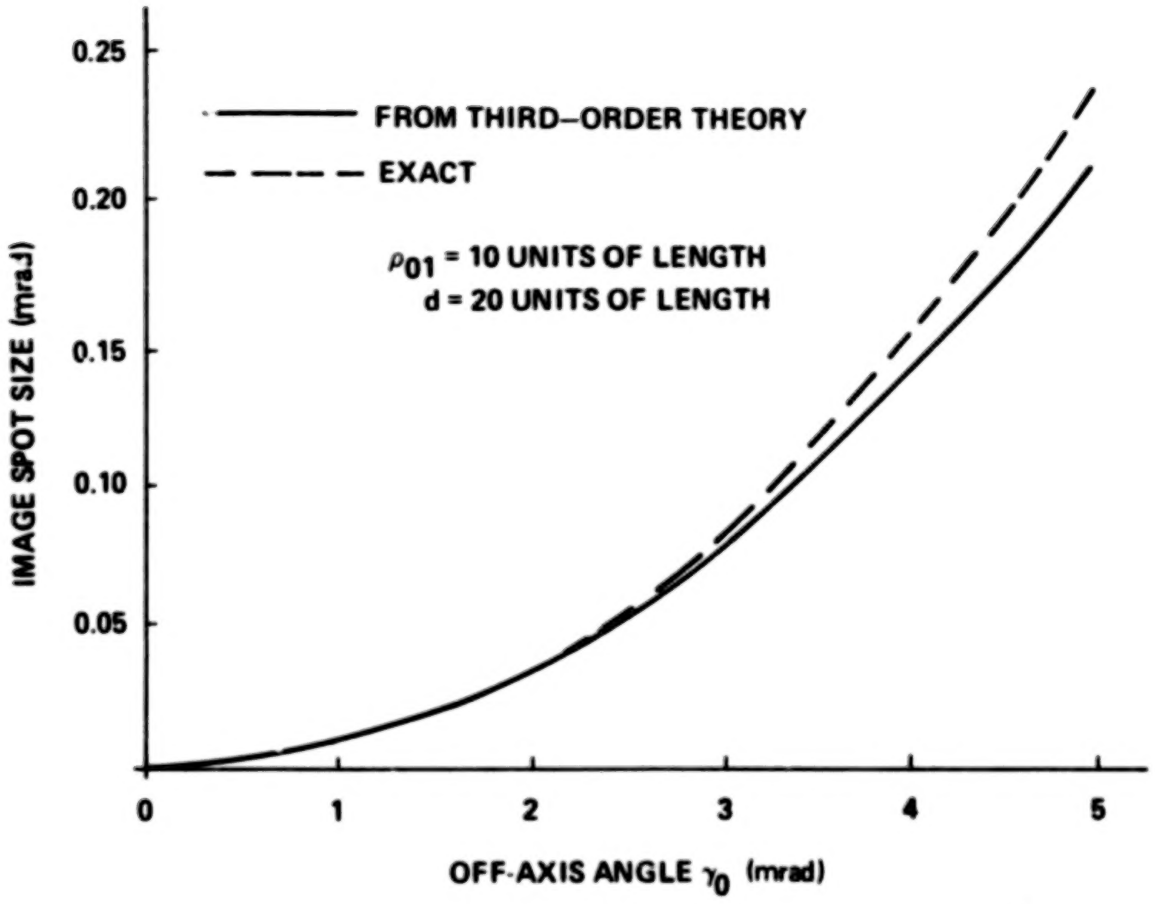

Figure 7. Exact spot size of image and spot size predicted by third-order theory versus off-axis angle.

V. CONCLUSIONS

It is believed that the choice of the coordinate system as discussed in Section IV is well justified by the results obtained. The origin was selected to coincide with the most representative portions of the reflecting surfaces, a thin ring located in the neighborhood of $z = 0$. The theory is thus most accurate for reflections occurring near the center of each element, and the distance between element centers has been shown to be an important parameter.

A complete set of primary aberrations has been derived for a single-element and for a two-element grazing incidence system. Field curvature has

been identified as the predominant primary aberration for the two-element system. It has been shown quantitively, by the telescope design example in Section IV, that the value of field curvature from this theory agrees to within better than 1 percent with the exact field curvature determined by ray-trace methods.

The primary aberrations have been discussed here; however, it was found that higher-order aberrations exist and become important at points of reflection outside the vicinity of the $z = 0$ plane.

REFERENCES

1. Wolter, H.: Spiegelsysteme streifenden Einfalls als abbildende Optiken für Röntgenstrahlen. Ann. Phys., vol. 10, 1952, p. 94.

2. Wolter, H.: Verallgemeinerte Schwarzschildsche Spiegelsysteme streifender Reflexion als Optiken für Röntgenstrahlen. Ann. Phys., vol. 10, 1952, p. 286.

3. Wolter, H.: Bildfehlerabschätzung für Röntgenstrahlenteleskope. Opt. Acta, vol. 18, 1971, p. 425.

4. Werner, W.: Imaging Properties of Wolter I Type X-Ray Telescopes. Appl. Opt., vol. 16, 1977, p. 764.

5. Winkler, C. and Korsch, D.: Primary Aberrations for Grazing Incidence. Appl. Opt., vol. 16, 1977, p. 2464.

6. Winkler, C.: Primary Aberrations for Grazing Incidence. Doctoral Dissertation, University of Alabama, May 1977.

7. Korsch, D.: Imaging Analysis of Mirrors from Normal to Grazing Incidence. J. Opt. Soc. Am., vol. 66, 1976, p. 938.

8. Schwarzschild, K.: Untersuchungen zur geometrischen Optik, I. Astr. Mitth. Königl. Sternw. Göttingen, 1905.

9. Giacconi, R. and Rossi, B.: A 'Telescope' for Soft X-Ray Astronomy. J. Geophys. Res., vol. 65, 1960, p. 773.

10. Giacconi, R., Harmon, N. H., Lacey, R. F., and Szilagyi, Z.: Aplanatic Telescope for Soft X-Rays. J. Opt. Soc. Am., vol. 55, 1965, p. 345.

11. Mangus, J. D. and Underwood, J. H.: Optical Design of a Glancing Incidence X-Ray Telescope. Appl. Opt., vol. 8, 1969, p. 95.

12. Van Speybroeck, L. P. and Chase, R. C.: Design Parameters for Paraboloid-Hyperboloid Telescopes for X-Ray Astronomy. Appl. Opt., vol. 11, 1972, p. 440.

REFERENCES (Concluded)

13. Chase, R. C. and Van Speybroeck, L. P.: Wolter-Schwarzschild Telescopes for X-Ray Astronomy. Appl. Opt., vol. 12, 1973, p. 1042.

14. Weisskopf, M. C.: Design of Grazing-Incidence X-Ray Telescopes. Appl. Opt., vol. 12, 1973, p. 1430.

APPROVAL

PERFORMANCE ANALYSIS OF GRAZING INCIDENCE IMAGING SYSTEMS

By Carl E. Winkler and Dietrich Korsch

The information in this report has been reviewed for security classification. Review of any information concerning Department of Defense or Atomic Energy Commission programs has been made by the MSFC Security Classification Officer. This report, in its entirety, has been determined to be unclassified.

This document has also been reviewed and approved for technical accuracy.

RUDOLF DECHER
Chief, Space Physics Division

CHARLES A. LUNDQUIST
Director, Space Sciences Laboratory

1. REPORT NO.	2. GOVERNMENT ACCESSION NO.	3. RECIPIENT'S CATALOG NO.
NASA TP-1088		

4. TITLE AND SUBTITLE	5. REPORT DATE
Performance Analysis of Grazing Incidence Imaging Systems	November 1977
	6. PERFORMING ORGANIZATION CODE

7. AUTHOR(S)	8. PERFORMING ORGANIZATION REPORT #
Carl E. Winkler and Dietrich Korsch*	M-241

9. PERFORMING ORGANIZATION NAME AND ADDRESS	10. WORK UNIT NO.
George C. Marshall Space Flight Center Marshall Space Flight Center, Alabama 35812	11. CONTRACT OR GRANT NO.
	13. TYPE OF REPORT & PERIOD COVERED
12. SPONSORING AGENCY NAME AND ADDRESS	Technical Paper
National Aeronautics and Space Administration Washington, D.C. 20546	14. SPONSORING AGENCY CODE

15. SUPPLEMENTARY NOTES

*Affiliated with Teledyne Brown Engineering, Huntsville, Alabama
Prepared by Space Sciences Laboratory, Science and Engineering

16. ABSTRACT

An exact expression relating the coordinates of a point on the incident ray, a point of reflection from an arbitrary surface, and a point on the reflected ray is first derived. The exact relation is then specialized for the case of grazing incidence, and first-order and third-order systematic analyses are carried out — first for a single reflective surface and then for a combination of two surfaces. The third-order treatment yields a complete set of primary aberrations for single-element and two-element systems. The importance of a judicious choice for a coordinate system in showing field curvature to clearly be the predominant aberration for a two-element system is discussed. The validity of the theory is verified through comparisons with the exact ray-trace results for the case of the telescope.

17. KEY WORDS	18. DISTRIBUTION STATEMENT
Grazing incidence Aberrations X-ray telescopes	Category 74

19. SECURITY CLASSIF. (of this report)	20. SECURITY CLASSIF. (of this page)	21. NO. OF PAGES	22. PRICE
Unclassified	Unclassified	39	$4.00

* For sale by the National Technical Information Service, Springfield, Virginia 22161

NASA-Langley, 1977